

Exploiting magnetic properties of Fe doped in zirconia

From first-principles simulations to the experimental growth and characterization of thin films.

D. Sangalli^{1,a}, E. Cianci¹, A. Lamperti¹, R. Ciprian¹, F. Albertini², F. Casoli², P. Lupo², L. Nasi², M. Campanini², and A. Debernardi¹

¹ Laboratorio MDM - IMM - CNR via C. Olivetti, 2 I-20864 Agrate Brianza (MB) Italy

² IMEM-CNR, Parco delle Scienze 37/A 43124, Parma, Italy

Abstract. In this study we explore, both from theoretical and experimental side, the effect of *Fe* doping in ZrO_2 ($ZrO_2:Fe$). By means of first principles simulation we study the magnetization density and the magnetic interaction between *Fe* atoms. We also consider how this is affected by the presence of oxygen vacancies and compare our findings with models based on impurity band [1] and carrier mediated magnetic interaction [2]. Experimentally thin films ($\approx 20nm$) of $ZrO_2:Fe$ at high doping concentration are grown by atomic layer deposition (ALD). We provide experimental evidence that *Fe* is uniformly distributed in the ZrO_2 by transmission electron microscopy (TEM) and energy dispersive X-ray (EDX) mapping, while X-ray diffraction (XRD) evidences the presence of the fluorite crystal structure. Alternating gradient force magnetometer (AGFM) measurements show magnetic signal at room temperature, however with low magnetic moment per atom. Results from experimental measures and theoretical simulations are compared.

1 Introduction

Dilute magnetic semiconductors (DMS) are materials in which magnetic impurities are introduced in order to produce a magnetic ground state. These systems have received great attention in recent years, since the discovery of carrier induced ferromagnetism in $(In, Mn)As$ [3] and $(Ga, Mn)As$ [4], and are believed to be fundamental to fabricate spin-based electronic devices. Recently a new class of DMS has been investigated, namely DMS based on high- k oxides, i.e. dilute magnetic oxides (DMO), after the experimental evidence of room temperature magnetism in transition metals (TMs) doped zirconia [5,6,7,8] (ZrO_2), hafnia [9,10] (HfO_2), and titania [11,12] (TiO_2) and the theoretical prediction of high T_c in TMs doped ZrO_2 [13,14].

The understanding of DMS/DMO physical properties constitutes a challenge for the theory as the fundamental mechanism leading to ferromagnetic (FM) interaction between the dopants cannot be explained in terms of simple exchange mechanisms, at least at low doping concentration, being the latter often too short-ranged. Among the

^a e-mail: davide.sangalli@mdm.imm.cnr.it

other, two theoretical models have been proposed to describe FM effects: the first is based on the presence of impurity states in the crystal, impurity band model (IBM) [1], the other on carriers in spin polarized bands, carrier mediated model (CMM) [2] which is indeed a refined version of the Zener model.

From the experimental side the inclusion and influence of magnetic dopant, such as *Fe*, *Co*, *Ni* and *Mn*, is not clearly understood. Indeed, while several DMS/DMO have been predicted to have a Curie temperature (T_c) above room temperature, no experimental report of $T_c > 300K$ has been left unchallenged by other studies [15]. Moreover some results suggest that magnetic impurities act as paramagnetic (PM) centers with unusually long relaxation time [16], at least at very low doping concentrations.

In this manuscript we study iron doped zirconia ($ZrO_2:Fe$) focusing our attention on the magnetic properties of the system. In Sec. 2 we provide a structural characterization of thin films grown by ALD. In particular we show that the doping is uniform, with high iron concentration and no segregation, and that zirconia is in the tetragonal/cubic structure. Thus theoretically we focus our attention on the tetragonal structure of zirconia with substitutional iron doping uniformly distributed in the sample. In Sec. 3 we study the magnetization of the system and how it is influenced by defects, i.e. oxygen vacancies (V_O), comparing our results with the IBM and the CMM. Indeed in a recent work we showed that iron doping induces V_O , with a ratio $y_{V_O/Fe} = 0.5$, for charge compensation, and that $ZrO_2:Fe$ films growth by ALD presents a ratio close to one half [17]. We finally investigate the magnetization of the films growth by ALD. From the magnetization at saturation we extract the magnetic moment per atom which is discussed in view of the results from theoretical simulations.

2 Structural Properties of $ZrO_2:Fe$

In order to describe the effect of iron doping in zirconia, $ZrO_2:Fe$ thin films were grown on *Si/SiO₂* substrates in a flow-type hot wall atomic layer deposition reactor (ASM F120) starting from β -diketonates metalorganic precursors. Ozone was used as oxidizing gas in the reaction process. The *Fe* concentration in $ZrO_2:Fe$ films can be tuned tailoring the *Zr/Fe* precursors pulsing ratio. In the present work however we focused our attention on the high doping regime keeping the pulsing ratio fixed. The growth temperature was maintained at 350°C. After the deposition the films were annealed at 600°C in N_2 flux for 60s to study their thermal stability. Further details on the samples preparation can be found in Ref. [18].

Film crystallinity was checked by X-ray diffraction (XRD) at fixed grazing incidence angle $\omega = 1^\circ$ and using *Cu K α* ($\lambda = 0.154$ nm) monochromated and collimated X-ray beam (Italstructure XRD 3000, details on the measurements can be found in Ref. [19]). In the present work all measures shown are from the same film which we chose as representative of the high-doping concentration samples. Fig 1(a) shows that the films present a cubic/tetragonal crystalline structure with an estimated cell parameter, assuming a cubic cell, $a = 5.024$ Å with a contraction of about $(a_{exp} - a_{exp}^0)/a_{exp}^0 \approx -1.0\%$; here $a_{exp}^0 = 5.074$ is the lattice parameter measured for undoped ZrO_2 films. Theoretically we found, at $x = 25\%$, $(a_{theo} - a_{theo}^0)/a_{theo}^0 \approx -0.4\%$, with $a_{theo}^0 = 5.11$, the lattice parameter computed for ZrO_2 , while the tetragonal deformation reduces from 3.05% to $< 1\%$.

The samples were then characterized by TEM, performed by a JEOL 2200FS microscope equipped with a high-angle annular-dark-field (HAADF) detector, in-column energy filter and EDX spectrometer. The layered geometry of the samples is shown in fig. 1(b). The *Fe* atomic concentration measured by EDX is 25%, in

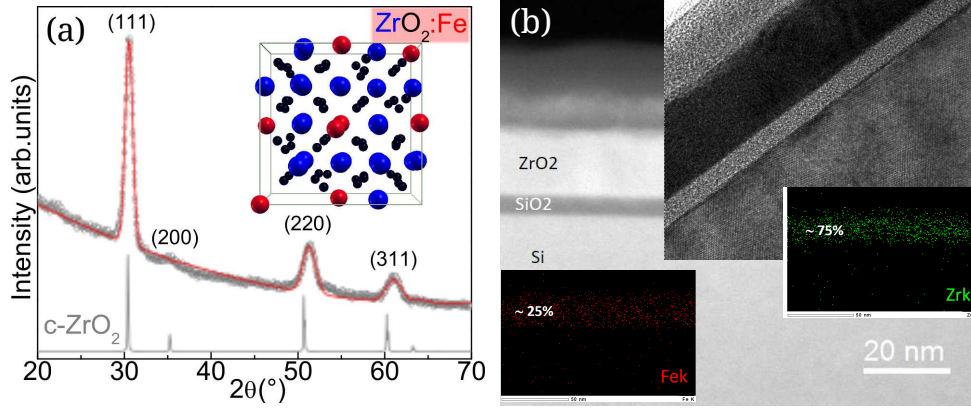


Fig. 1. (colors online) Structural properties of iron doped zirconia. Panel (a): XRD patterns show that the film presents the cubic/tetragonal phase [28]. A representation of the fully relaxed theoretical structure is also pictured with *Fe* atoms in red, *Zr* atoms in blue and oxygens in black (we used the Xcrysden software [29]). Panel (b): HAADF image and HREM inset showing the layered geometry of the sample. The EDX chemical maps show a uniform doping distribution with no segregation.

agreement within few percent to the estimation done by X-ray photo-emission (XPS). The EDX maps, taken in different regions of the samples, showed that *Fe* is uniformly distributed across the film and no clusters or segregation at the grain boundaries have been found (see Fig. 1(b), insets).

Thus theoretically we computed, from first-principles, the ground state of the the tetragonal phase of $ZrO_2:Fe$ with uniform iron doping distribution. We used the PWSCF [20] package considering a super-cell with 96 atoms; for all systems the atomic positions are fully relaxed [21]. The ground state was computed with the generalized gradient approximation [22] (GGA) to the density functional theory (DFT) scheme [23,24] with ultra-soft pseudo-potentials [25,26]. We have recently shown that iron, in the zirconia host lattice, behave like Yttrium (*Y*) which is among the most studied dopant of this oxide: it replaces zirconium atoms in the ZrO_2 lattice inducing V_O for charge compensation, with a ratio $y_{V_O/Fe} = 0.5$, and stabilizes the tetragonal phase above $x_{Fe} \approx 11\%$ [27,17]. Calculations have been done at different doping concentrations, $x_{Fe} = 6.24, 12.5, 25.0\%$ and different V_O concentration, considering the V_O to *Fe* ratios $y_{V_O/Fe} = 0, 0.5, 1$, focusing our attention at the high doping concentration limit, i.e. the concentration measured experimentally. In the inset of Fig. 1(b) a relaxed structure at $y_{V_O/Fe} = 0.5$ and $x_{Fe} = 25\%$, which is the expected structure in our films [17], is shown.

3 Magnetic Properties of $ZrO_2:Fe$

Starting from the fully relaxed structures considered at $x_{Fe} = 25\%$ we computed the local magnetization of the system. In Fig. 2 the magnetization density, i.e. the difference between the spin-majority and the spin-minority density is represented for $y_{V_O/Fe} = 0, 0.5, 1$. In order to compare the present results with the IBM also the total density of states (DOS) are plotted. The FM configuration is considered for better clarity as it helps to distinguish between the minority and the majority spin channel. However all the conclusion we will draw in the following also hold for the

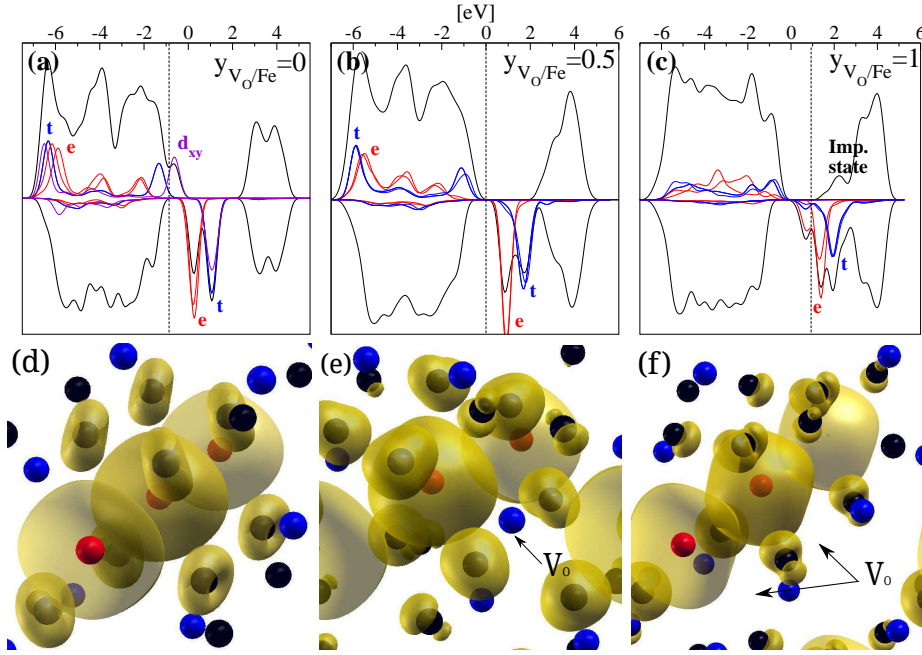


Fig. 2. (colors online) Theoretical density of states (panels *a-c*) and magnetization density isosurfaces at $m = 0.01$ a.u. (panels *d-f*) for the ferromagnetic configuration at $y_{V_O/Fe} = 0, 0.5, 1$. The density of states projected on the d atomic orbitals is also shown. The crystal field splitting is visible with the e doublet, d_{z^2} and $d_{x^2-y^2}$ in blue, at higher (lower) energy in the majority (minority) spin channel respect to the t triplet, d_{xy} , d_{xz} and d_{yz} in red. In panels *d-f* Fe atoms are represented in red, Zr atoms in blue and oxygens in black.

anti-FM configuration (see Fig. 3(*b-c*)) for a comparison of the anti-FM magnetization density).

At $y_{V_O/Fe} = 0$, the system shows holes in the valence band (Fig. 2(*a*)) because iron act as an acceptor; the projected DOS shows that these are localized on the $Fe(d_{xy})$ level. As a consequence the majority-spin d band is not completely filled, the magnetic moment per iron atom is $4 \mu_B$ and iron is forced in a +4 oxidation state. This also breaks the spherical symmetry of the system and the shape of the magnetization density close to the oxygens is not isotropic, with a peculiar doughnut shape oriented in the xy -plane.

Creating V_O , i.e. increasing $y_{V_O/Fe} > 0$, electrons are released in the system. These fill the empty d_{xy} levels with a charge-transfer mechanism. At $y_{V_O/Fe} = 0.5$ the majority d band is completely filled, the magnetic moment per iron atom is $5 \mu_B$ and the magnetization has a spherical shape. The system turns into a charge-transfer semi-conductor (Fig. 2(*b*)). At $y_{V_O/Fe} = 1$ electrons fill the minority d levels and the magnetic moment per iron atom is reduced to $4 \mu_B$. However the minority d electron does not participate in the bonds, thus the anisotropy is only weakly transferred to the p orbitals of oxygen (Fig. 2(*c*)). In all configurations the magnetization is mainly located around the Fe atoms and it is in part transferred to the oxygen next nearest neighbor suggesting a short range magnetic interaction (Fig. 2(*d-f*)).

It is worth to compare the DOS of our system with the IBM. A crucial assumption of the IBM is that the presence of V_O creates impurity states with poorly localized electrons. These, already at low doping concentration, would overlap to create an

impurity band that can mediate the FM interaction among nearby iron atoms. Indeed V_O are a common defect in pure ZrO_2 films where they create impurity states close to the conduction band, however in the case for $ZrO_2:Fe$ the situation is different, as shown in Fig. 2(a-c). For low V_O concentration, i.e. $y_{V_O/Fe} \leq 0.5$ no impurity states are associated to V_O while for $x > 0.5$ impurity states appear but higher in energy than the empty spin minority d -levels. Thus the extra electrons are trapped in the $Fe(d)$ levels and the impurity states remain empty. More in general, the majority of magnetic transition metals (TMs), i.e. Fe , Co , Ni , Mn , and Cr , have +2 or +3 as most stable oxidation state and we expect a similar picture for all TMs doped XO_2 oxides, at least for $y_{V_O/Fe} \leq 0.5$ (1.0), in the case of +3 (+2) oxidation state. Thus, according to our results, the IBM cannot be invoked to describe the magnetic ground-state for $ZrO_2:Fe$ and for $XO_2:TM$ in general.

The situation depicted is much closer to the CMM proposed for $Ga_{1-x}Mn_xAs$. In $Ga_{1-x}Mn_xAs$ Mn acts as an acceptor which compensates the antisite defects commonly present in $GaAs$ giving a charge-transfer semiconductor; in $ZrO_2:Fe$ Fe acts as an acceptor compensating the V_O . The main difference between the two systems is the nature of the host lattice, a covalent semiconductor the former and a polar oxide the latter. In $Ga_{1-x}Mn_xAs$, when x_{Mn} exceeds the antisite defect concentration, the system behaves like a metal with holes in the valence band. In $ZrO_2:Fe$ instead, at $y_{V_O/Fe} \leq 0.5$, the holes locate onto the d_{xy} states (see Fig. 2(b)); conduction could be possibly obtained only at high doping concentration with a hopping like mechanism.

We finally focus our attention on more standard exchange mechanisms studying the energy of the magnetic interaction in our system. This in principle can be computed as the energy difference between the FM and the PM phase. The latter however can be hardly described within a periodic code, as the description of random magnetic moment orientations would require huge supercells with a non-collinear description of the wave-functions. The energy difference per iron atom between the FM and the anti-FM configuration however can be used as a reasonable approximation [15]. We found that at lower doping, $x_{Fe} = 6.25, 12.5\%$, the energy difference is very low with $\Delta E/k_B$ of the order of few kelvin [30]. The anti-FM configuration is slightly favored at $y_{V_O/Fe} = 0.5$, while the FM one is slightly favored at $y_{V_O/Fe} = 0$. Instead at $x_{Fe} = 25\%$ in both cases the anti-FM configuration is favored with $\Delta E/k_B \approx 150K$ for $y_{V_O/Fe} = 0.5$ and $\Delta E/k_B \approx 20K$ for $y_{V_O/Fe} = 0$. This suggests a short range interaction which becomes relevant at $x_{Fe} > x_P$, with x_P the percolation threshold, i.e. an anti-FM super-exchange mechanism which is dominant in the $y_{V_O/Fe} = 0.5$ case. For the $y_{V_O/Fe} = 0$ configuration however this super-exchange mechanism appears to be in competition with a FM interaction which could be explained in terms of the CMM model, though with a weaker effect due to the low mobility of the holes. This results in a weakly FM interaction at low doping and a weakly anti-FM interaction at higher doping.

The magnetic properties of sample with $x_{Fe} \approx 25\%$ were studied by means of alternated gradient force magnetometry (AGFM). Magnetization measurements, performed at room temperature by applying the magnetic field parallel to the film plane, show a clear hysteresis loop characterized by a coercive field $\mu_0 H_c \approx 0.03 T$ (Fig. 3(a)). From the saturation magnetization value a magnetic moment per Fe atom $m \approx 0.6\mu_B$ can be extrapolated. This is consistent with the values reported in the literature but is one tenth of the theoretically predicted value, $m \approx 5\mu_B$. Moreover theoretically we found that the anti-FM configuration is the most stable at least for $y_{V_O/Fe} = 0.5$ which is the expected situation in our films [17]. In Fig. 3(b-c) we plotted the magnetization density in the anti-FM configuration for $y_{V_O/Fe} = 0.5$. As in the case of FM ground state, the magnetization is mainly located on the Fe atoms and the next nearest neighbor oxygens.

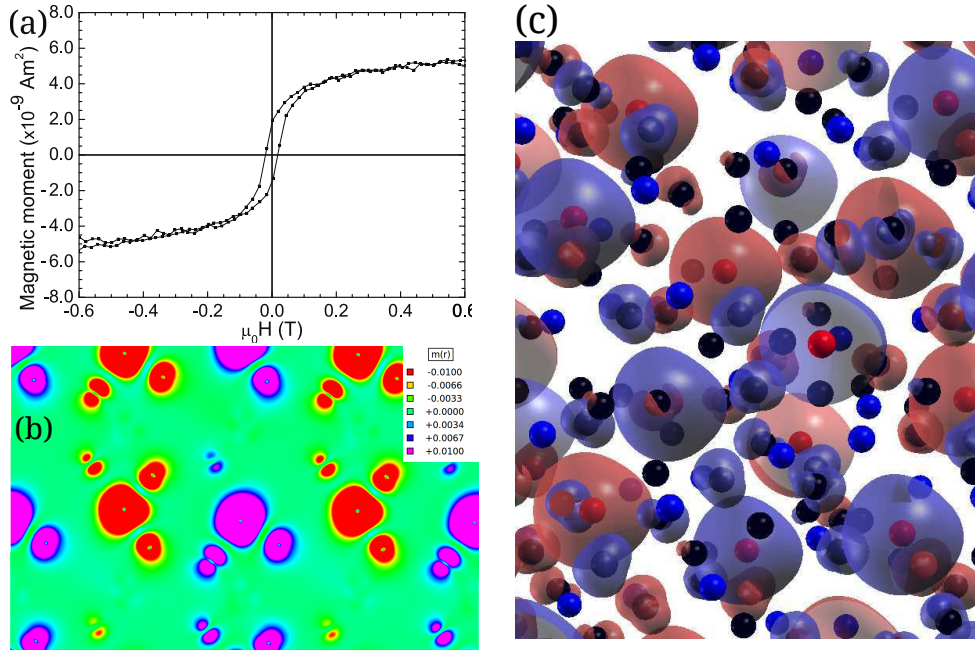


Fig. 3. (colors online) Panel *a*: magnetization hysteresis loop measured by AGFM at room temperature. The resulting magnetization at saturation can be interpreted in terms of a anti-ferromagnetic structure if $y_{V_O/Fe}$ deviates from 0.5 of about 10%. The magnetization density for the anti-FM configuration at $y_{V_O/Fe} = 0.5$ is plotted in panels (b)-(c). Panel *b*: 2D contour plot of the magnetization density along the plane (1 -1 0). Panel *c*: Positive (red) and negative (blue) isosurfaces of the magnetization density at $m = \pm 0.02$.

The discrepancy between the theoretically and the experimental results could be possibly explained supposing that experimentally $y_{V_O/Fe} = 0.5$ were not fulfilled by few percent of the Fe atoms, which thus would be in the Fe^{4+}/Fe^{2+} oxidation state. If we assume that these ions would couple with FM interaction, with a CMM like mechanism, the net results would be a weak magnetic system with low magnetic moment per atom. However further investigations are needed, both experimentally and theoretically, to clarify this point.

4 Conclusions

In conclusion we have studied both theoretically and experimentally thin films of iron doped ZrO_2 . Experimentally we have shown that iron distributes uniformly at high doping concentration with no cluster formation and that the system is magnetized at room temperature. With first principles simulations we have discussed the possible magnetization mechanisms comparing our results with other model proposed in the literature. We showed that the impurity band model cannot be invoked in the case of iron doped zirconia while the carrier mediated model could be possibly considered for uncompensated oxygen vacancies concentration (i.e. $y_{V_O/Fe} \neq 0.5$). The standard super-exchange mechanism however appears to be dominant for $y_{V_O/Fe} = 0.5$.

From magnetization measurements of highly doped samples we found a low saturation magnetization value corresponding to low magnetic moment per Fe atom. We tried to interpret the experimental results in view of our theoretical findings. However the difference between theory and experiments suggest that other effects need to be taken into account for a correct description of the magnetic properties of the system.

5 Acknowledgements

This work was funded by the Cariplo Foundation through the OSEA project (n. 2009-2552). Helpful discussions with L. Lazzarini are gratefully acknowledged. D.S. and A.D. would like to acknowledge G. Onida and the ETSF Milan node for the opportunity of running simulations on the “etsfmi cluster”, and P. Salvestrini for technical support on the cluster. We also acknowledge computational resources provided by the Consorzio Interuniversitario per le Applicazioni di Supercalcolo Per Università e Ricerca (CASPUR) within the project MOSE.

References

1. J. M. D. Coey, M. Venkatesan, and C. B. Fitzgerald, *Nature Materials* **4**, (2005) 173
2. T. Dietl, H. Ohno, F. Matsukura, J. Cibert, and D. Ferrand, *Science* **287**, (2000) 1019
3. H. Ohno, H. Munekata, T. Penny, S. Von Molnar, and L. L. Chang, *Phys. Rev. Lett.* **68**, (1992) 2664
4. H. Ohno, A. Shen, F. Matsukura, A. Oiwa, A. Endo, S. Katsumoto and Y. Iye, *Phys. Rev. Lett.* **69**, (1996) 363
5. N. H. Hong, C.-K. Park, A. T. Raghavender, O. Ciftja, N. S. Bingham, M. H. Phan, and H. Srikanth, *J. Appl. Phys.* **111**, (2012) 07C302
6. J. M. D. Coey, M. Venkatesan, P. Stamenov, C. B. Fitzgerald, L. S. Dorneless, *Phys. Rev. B* **72**, (2005) 024450
7. T. R. Sahoo, S. S. Manoharan, S. Kurian, and N. S. Gajhiye, *Hyperfine Interaction* **188**, (2009) 43
8. V. V. Kriventsov, D. I. Kochubey, Y. V. Maximov, I. P. Suzdalev, M. V. Tsodikov, J. A. Navio, M. C. Hidalgo, G. Colón, *Nuclear Instruments and Methods in Physics Research A* **470**, (2001) 341
9. N. H. Hong, J. Sakai, N. Poirrot, and A. Ruyter, *Appl. Phys. Lett.* **86**, (2005) 242505
10. N. H. Hong, N. Poirrotet, and J. Sakai, *Appl. Phys. Lett.* **89**, (2006) 042503
11. Y. Matsumoto, et al., *Science* **291**, (2001) 854
12. Z. J. Wang, K. J. Tang, L. D. Tung, W. L. Zhou, and L. Spinu, *J. Appl. Phys.* **93**, (2003) 7870
13. S. Ostanin, A. Ernst, L. M. Sandratskii, P. Bruno, M. Däne, I. D. Hughes, J. B. Staunton, W. Hergert, I. Mertig, and J. Kudrnovský *Phys. Rev. Lett.* **98**, (2007) 016101
14. T. Archer, C. D. Pemmaraju, and S. Sanvito, *Journal of Magnetism and Magnetic Materials* **316**, (2007) e188-e190
15. K. Sato, L. Bergqvist, J. Kudrnovsky, P. H. Dederichs, O. Eriksson, I. Turek, B. Sanyal, G. Bouzerar, H. Katayama-Yoshida, V. A. Dinh, T. Fukushima, H. Kizaki, R. Zeller, *Rev. Mod. Phys.* **82**, (2010) 1633
16. H. P. Gunnlaugsson, T. E. Mlholt, R. Mantovan, H. Masenda, D. Naidoo, W. B. Dlamini, R. Sielemann, K. Baruth-Ram, G. Weyer, K. Johnston, G. Langouche, S. Olafsson, H. P. Gislason, Y. Kobayashi, Y. Yoshida, M. Fanciulli, and ISOLDE Collaboration, *Appl. Phys. Lett.* **97**, (2010) 142501
17. D. Sangalli, E. Cianci, R. Ciprian, A. Lamperti, M. Perego and A. Debernardi, arXiv:1206.1197v1
18. A. Lamperti, E. Cianci, R. Ciprian, D. Sangalli, and A. Debernardi, arXiv:1206.2857v1

19. A. Lamperti, L. Lamagna, G. Congedo, and S. Spiga, J. Electrochem. Soc., **158**, (2011) G211
20. P. Giannozzi, S. Baroni, N. Bonini, M. Calandra, R. Car, C. Cavazzoni, D. Ceresoli, G. L. Chiarotti, M. Cococcioni, I. Dabo, A. Dal Corso, S. Fabris, G. Fratesi, S. de Gironcoli, R. Gebauer, U. Gerstmann, C. Gougoussis, A. Kokalj, M. Lazzeri, L. Martin-Samos, N. Marzari, F. Mauri, R. Mazzarello, S. Paolini, A. Pasquarello, L. Paulatto, C. Sbraccia, S. Scandolo, G. Sclauzero, A. P. Seitsonen, A. Smogunov, P. Umari, R. M. Wentzcovitch, J. Phys.:Condens. Matter **21**, (2009) 395502; <http://www.quantum-espresso.org>
21. We use a cut—off of 35 Ry for the wave—functions and 400 Ry for the augmentation density; a Monkhorst—Pack grid 2x2x2 for the Brillouin zone.
22. J. P. Perdew, K. Burke, and M. Ernzerhof, Phys. Rev. Lett. **77**, (1996) 3865
23. P. Hohenberg, and W. Kohn, Phys. Rev. **136**, (1964) B864
24. W. Kohn, and L. J. Sham, Phys. Rev. **140**, (1965) A1133
25. D. Vanderbilt, Phys. Rev. **B 41**, (1990) 7892R
26. A. M. Rappe, K. M. Rabe, E. Kaxiras, and J. D. Joannopoulos, Phys. Rev. **B 41**, (1990) 1227R
27. D. Sangalli, and A. Debernardi, Phys. Rev. **B 84**, (2011) 214113
28. International Crystal Structure Database, FIZ Karlsruhe and NIST ed., Release 2010 Code #68589 (t-ZrO₂)
29. A. Kokalj, Comp. Mater. Sci. **28**, 155 (2003)
30. The ferromagnetic structure at $x_{Fe} = 12.5\%$ is frustrated. Considering the closest Fe - Fe atoms we have in total, within in the supercell, 6 anti-ferromagnetic “connections” and 2 ferromagnetic connections.